European Fate Of Repository Gases Project: Final report on numerical simulations of gaz and water flow in clay with Code_Aster; PGZ1 modelling

FORGE Report D4.21– VER.0

	Name	Organisation	Signature	Date
Compiled	Granet Sylvie	EDF		20/12/12
Verified	Fernandes Roméo	EDF		
Approved	RP Shaw	BGS		19 November 2013

Keywords :

FORGE Experiment, Hydro-mechanical coupling, two-phase flow model, Code_Aster numerical simulation.

Euratom 7th Framework Programme Project: FORGE

Fate of repository gases (FORGE)

The multiple barrier concept is the cornerstone of all proposed schemes for underground disposal of radioactive wastes. The concept invokes a series of barriers, both engineered and natural, between the waste and the surface. Achieving this concept is the primary objective of all disposal programmes, from site appraisal and characterisation to repository design and construction. However, the performance of the repository as a whole (waste, buffer, engineering disturbed zone, host rock), and in particular its gas transport properties, are still poorly understood. Issues still to be adequately examined that relate to understanding basic processes include: dilational versus visco-capillary flow mechanisms; long-term integrity of seals, in particular gas flow along contacts; role of the EDZ as a conduit for preferential flow; laboratory to field up-scaling. Understanding gas generation and migration is thus vital in the quantitative assessment of repositories and is the focus of the research in this integrated, multi-disciplinary project. The FORGE project is a pan-European project with links to international radioactive waste management organisations, regulators and academia, specifically designed to tackle the key research issues associated with the generation and movement of repository gasses. Of particular importance are the long-term performance of bentonite buffers, plastic clays, indurated mudrocks and crystalline formations. Further experimental data are required to reduce uncertainty relating to the quantitative treatment of gas in performance assessment. FORGE will address these issues through a series of laboratory and field-scale experiments, including the development of new methods for up-scaling allowing the optimisation of concepts through detailed scenario analysis. The FORGE partners are committed to training and CPD through a broad portfolio of training opportunities and initiatives which form a significant part of the project.

Further details on the FORGE project and its outcomes can be accessed at www.FORGEproject.org.

Contact details:

[1]

Author 1 Granet Sylvie

Organisation EDF

EDF R&D

Analysis in Mechanics and Acoustics (AMA)

Tel: +33 (0)1.47.65.50.15 Fax +33 (0)1.47.65.41.18

email: sylvie.granet@edf.fr

Address 1, avenue du Général de Gaulle – 92.140 Clamart – France.

Contents

1. Introduction 1

2. A Brief description of PGZ1 experiment 2

2.1 General configuration 2

2.1 Experimental observations 4

3. Description of numerical software Code_Aster and its conceptual models 6

3.1 Model used in this study 6

3.2 Some numerical aspects.....9

4. Material data 9

4.1 Argilite.....9

4.2 Injection chamber PRE02 (Interval 2).....10

4.3 Liquid and gas parameters 11

5. First set of hypothesis of numerical simulation 11

5.1 Geometry and mesh 11

5.2 Initial conditions 13

5.3 Steps of simulation and boundary conditions.....14

5.4 Experimental curve correction.....16

5.5 3D computation 17

5.6 Axisymetric computations 21

6. Second set of hypothesis of numerical simulations: taken into account of the initial saturation of the injection interval 28

6.1 Some elements concerning the volume of the injection's chamber 28

6.2 New Hypothesis of computation 29

6.3 Reference computation 29

6.4 Introduction of a borehole damage zone 31

6.5 Goal of gas permeability in host rock.....32

7. Conclusions 33

8. References 34

Annexe 1 35

Figures

Figure 1 – PGZ1 experiment configuration 3

Figure 2 – Around gas injection chamber PRE02 3

Figure 3 – Phases of PGZ1 experiment 4

Figure 4 – *Water pressure and gas fluxes in PGZ1201* 5

Figure 5 - *Water pressure and gas fluxes in PGZ1201 - Zoom on gas injection phase* 5

Figure 6 – *Water pressure in PGZ1202* 6

Figure 7 – *3D geometry with orange circled injection chamber* 12

Figure 8 – *Zoom of injection chamber* 12

Figure 9 - *Orientation of the borehole* 13

Figure 10 – *2D geometry with orange colored injection chamber* 13

Figure 11 – *Experimental Pressure evolution for HYDRO1 Phase in injection chamber* 17

Figure 12 – *Corrections of experimental Pressure measurement in injection chamber during GAS1* 17

Figure 13 - *Measurement points* 18

Figure 14 - *Liquid pressure evolution* 19

Figure 15- *Liquid pressure evolution, zoom on GAS1 phase* 19

Figure 16 - *Numerical saturation evolution* 19

Figure 17 - *Liquid pressure isovalue at t = GRI1* 20

Figure 18 - *Liquid pressure isovalue at t = GRI3* 20

Figure 19 - *Liquid pressure isovalue at t = GRI4* 21

Figure 20- *Liquid pressure isovalue at t = GRI5* 21

Figure 21 - *Point and line of post-processing on 2D model* 22

Figure 22 - *Liquid pressure evolution on PRE02* 23

Figure 23 - *Saturation evolution on PRE02* 23

Figure 24 - *Total radial stresses at several times along L* 24

Figure 25- *Plastic strain at several times along L* 24

Figure 26- *Liquid Pressure at several times along L* 24

Figure 27- $\chi_l^{N_2}$ *(Gas pressure or concentration) at several times along L* 25

Figure 28- *Liquid Saturation at several times along L* 25

Figure 29 $\chi_l^{N_2}$ *isovalues (zoom around the chamber)* 26

Figure 30 - *Influence of chamber compressibility* 26

Figure 31 - *Influence of undisturbed rock intrinsic permeability* 27

Figure 32 - *Modification of rock permeability after GRI3* 28

Figure 33 – *Interval 2 (injection chamber)* 28

Figure 34 – *Gas pressure evolution in interval 2: goal of initial saturation* 30

Figure 35 – $\chi_l^{N_2}$ *(Gas pressure or concentration) at several times along L* 30

Figure 36 – *Liquid Saturation at several times along L* 31

Figure 38 – *Gas/liquid ration of Nitrogen at several times along L* 31

Figure 40 –*Configuration and hypothesis of modeled BDZ*.....32

Figure 41 – *Gas pressure evolution in interval 2: goal of BDZ* 32

Figure 46 – *Gas pressure evolution in interval 2 : goal of relative permeability in host rock* 33

Summary

This report gives numerical interpretations of PGZ1 experiment led by ANDRA in experimental laboratory of Bure. The results presented here are obtained by EDF with Code_Aster. The main goal of this in situ experiment is to understand and quantify gas transfer mechanisms in callovo-oxfordian. More precisely, initial goal was to fit the parameters of gas transfer through medium and to verify that the expected mechanisms are observed: dissolution of nitrogen into water, appearance of the gas phase, and at least reach of micro-fracturation threshold. We propose in this report a fully coupled hydromechanical simulation of this experience.

In the first part of this document, we present briefly the PGZ1 experiment. Second part is dedicated to preliminary computations (2011). For that, hydromechanical computations taken into account the digging of the borehole have been done in 3D and 2D. At least, the third part is dedicated to axisymetric computations of injection phase only with a best approximation of initial gas volume in the interval chamber. In this part we highlight the importance of the different components of the experiment and not only undisturbed host rock. Major difficulty in in-situ test modeling is finally to understand and capture what happens in the instrumentation and not only in clay. Indeed, we will show here the importance of a precise modeling of injection interval: volume, initial saturation and physical characteristics. Moreover “damage rock” is studied. This area seems to play an important role but is hard to characterize.

By the way, we can more or less reproduce experiment and to understand phenomena but it seems still impossible to provide predictive modeling

1. Introduction

A great deal of attention is focused on radioactive waste management in nuclear industry and especially in the feasibility of deep geological underground disposal. A major issue concerns perturbations induced by the repository on the environment. In these deep geological disposals, an important phenomenon to be considered is the production of gas. Those gases (mostly hydrogen) are generated by radiolysis or anoxic corrosion of steel components. Consequences of hydrogen production could be high gas and water pressures, damage and modification of retention properties of the repository: the migration pathway for radionuclide could be modified. In order to assess feasibility of the deep geological disposal of radioactive waste, a large program of experiments, led by Andra, has been engaged at the Meuse/Haute-Marne research laboratory. PGZ1 is one of these experiments and is focused on perturbations induced by gas production in undisturbed clay.

Main goals of PGZ1 experiment are:

- Characterization of gas transfer through medium (through natural and modified clays, caps and interfaces)

- Validation of biphasic model and of its parameters (diffusion, capillary pressure, permeability)
- Estimation of micro-fracturation threshold

Further details about the experimental protocol are given in section 2. This experiment is still ongoing.

In FORGE project, two teams participate in PGZ1 numerical simulation:

- EDF with Code_Aster, since October 2010
- Université de Liège with Lagamine, since June 2010

In section 5, 2D and 3D numerical simulations of PGZ1 experiment are proposed with *Code_Aster*. In this section digging, hydraulic phase and gas injection phase are simulated. 3D computation has been done but is quite computationally expensive and do not bring significant novelties with respect to 2D modeling. With 2D axisymmetric simulation, a sensitivity analysis and some comparisons with experimental observations have been done: First part of experience is well reproduced but important differences are observed for the last part. In section 6, only gas injection phase is simulated and the initial saturation of injection chamber is well taken into account. 2D axisymmetric computations have been done under different configurations (presence or not of a borehole damage zone).

2. A Brief description of PGZ1 experiment

In this section, we describe PGZ1 experiment and we present experimental observations which are modelized in section 5 et 6. All the details of experiment are given in [1] and [4].

2.1 GENERAL CONFIGURATION

Figure 1 illustrates general configuration of PGZ1 experiment. From two main galleries (GED and GEX), 3 boreholes are drilled (PGZ1201, PGZ1202 and PGZ1031):

- PGZ1201 is used for gas injection (N_2) and is equipped with 3 chambers. In Annex 1, precise description of the installation is given. Full installation is a 28 m long cylinder and has a diameter of 0.076 m. Gas injection is realized through one meter long middle chamber PRE02. Zoom around this chamber is proposed in *Figure 2*. Packers (grey-colored) are water-saturated. Inter-packers (yellow-colored) are filled with resin.
- PGZ1202 is used for pressure observation and is also equipped with 3 chambers. It is almost parallel to PGZ1201.
- PGZ1031 is used for strain observation, with an extensometer with 20 measurement points. It is perpendicular to PGZ1201, one meter above. It will mainly be used to follow fracture opening in a later phase, after gas injection.

The objective is to follow the evolution of water pressure. We could wonder if presence of boreholes PGZ1202 and especially the nearest PGZ1031 could have an influence onto PGZ1201 chamber.

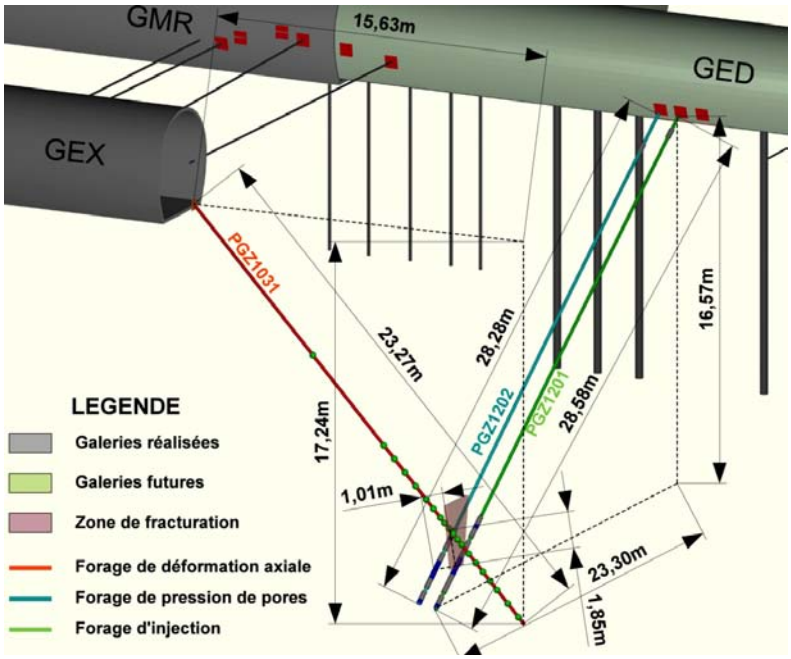

Figure 1 *– PGZ1 experiment configuration*

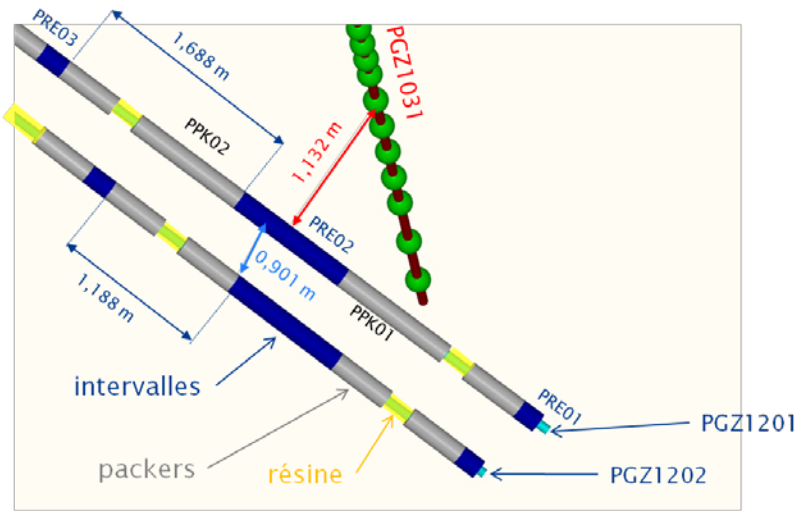

Figure 2 *– Around gas injection chamber PRE02*

A complete description of the experiment is given in the technical report [1], detailing each phase of equipment installation. General planning of experiment is described in the following table *Figure 3*. In the sequel, dates are expressed with the english convention.

time	borehole	description	phase	duration

				(days)
2009-07-02	PGZ1031	drilling PGZ1031		
2009-07-03	PGZ1031	equipment installation		
2009-07-27	PGZ1201	drilling PGZ1201		
2009-07-28	PGZ1201	equipment installation		
2009-07-29	PGZ1202	drilling PGZ1202		
2009-07-30	PGZ1202	equipment installation		
2009-08-28	PGZ1201	pulse	HYDRO1	
2009-09-14	PGZ1201	constant pressure test	HYDRO1	5
2010-01-28	PGZ1201	water-gas exchange (N_2)	Start GAS1	
2010-02-01	PGZ1201	start gas injection 1	GRI1	11
2010-02-05	PGZ1201	increase flowrate		
2010-02-12	PGZ1201	stop gas injection 1	GRIS1	19
2010-03-03	PGZ1201	start gas injection 2	GRI2	15
2010-03-18	PGZ1201	stop gas injection 2	GRIS2	20
2010-04-07	PGZ1201	start gas injection 3	GRI3	7
2010-04-14	PGZ1201	stop gas injection 3	GRIS3	28
2010-05-12	PGZ1201	start gas injection 4	GRI4	14
2010-05-25	PGZ1201	stop gas injection 4	GRIS4	29
2010-06-18	PGZ1201	packer inflation		
2010-06-24	PGZ1201	start gas injection 5	GRI5	11
2010-07-01	PGZ1201	flow gas controller failure		
2010-07-05	PGZ1201	stop gas injection 5	GRIS5	107
2010-10-20	PGZ1201	start gas injection 6	GRI6	15
2010-11-04	PGZ1201	stop gas injection 6	GRIS6	>117

Figure 3 *– Phases of PGZ1 experiment*

2.1 EXPERIMENTAL OBSERVATIONS

Gas (Nitrogen) production begins on 10/02/01 in central chamber PRE02. This injection, with constant fluxes, followed by stopping phases, is illustrated in purple in Figure 4. This figure also shows measured pressure in the 3 chambers (PRE01, PRE02, PRE03) of PGZ1201 during the experiment.

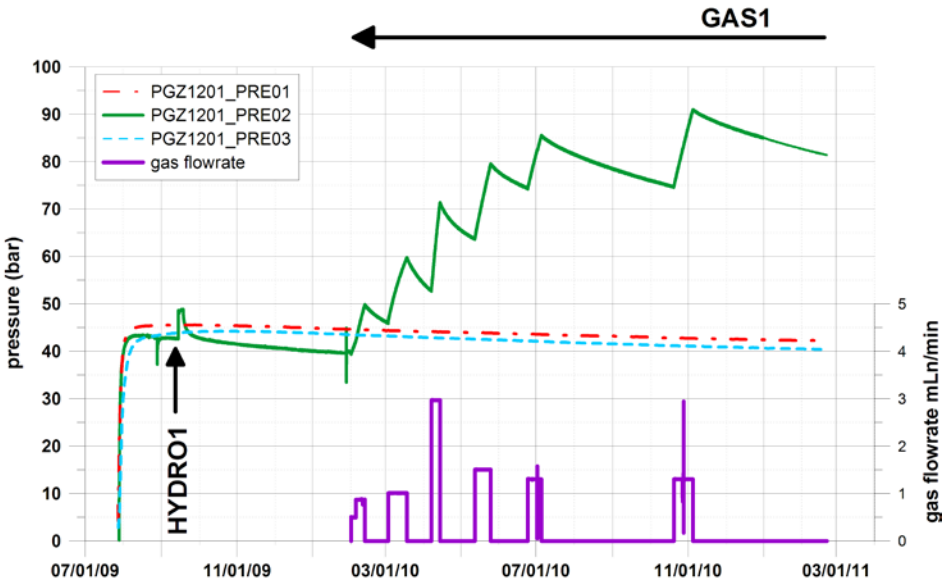

Figure 4 – *Water pressure and gas fluxes in PGZ1201*

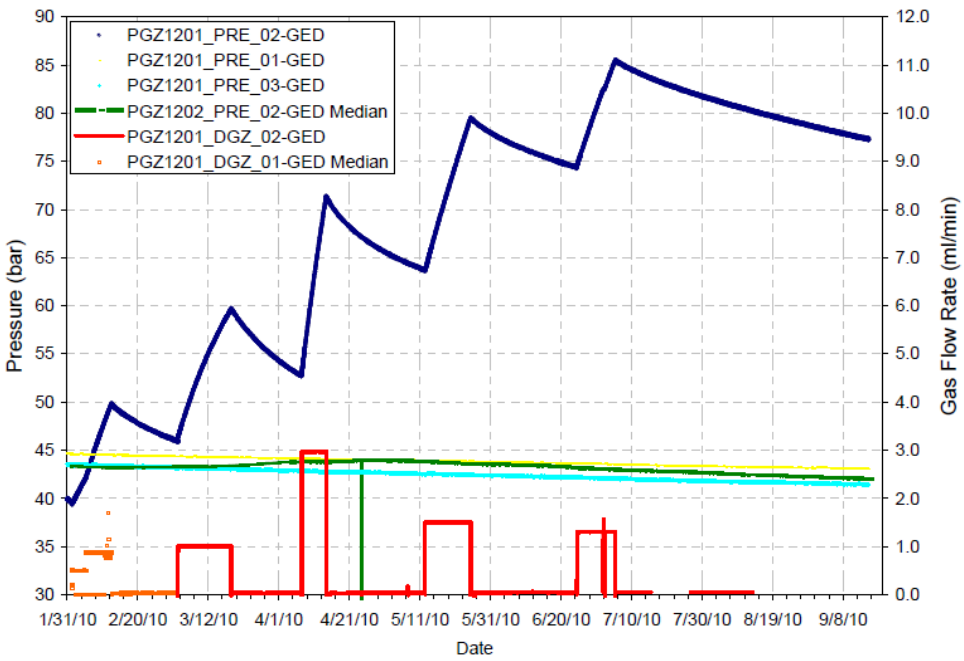

Figure 5 - *Water pressure and gas fluxes in PGZ1201 - Zoom on gas injection phase*

We observe that influence of gas injection in PRE02 into two chambers PRE01 and PRE03 is negligible. Therefore, it probably means that there is no significant Borehole Damage Zone due to drilling.

After HYDRO1 phase, there is a regular but unexplained decrease of water pressure. We expected pressure to be stable. Drainage by other borehole (PGZ1031) was suspected and has been confirmed by simulations of ULg.

During the GAS1 phase we observe the different steps of pressure increase according to gas flow injection.

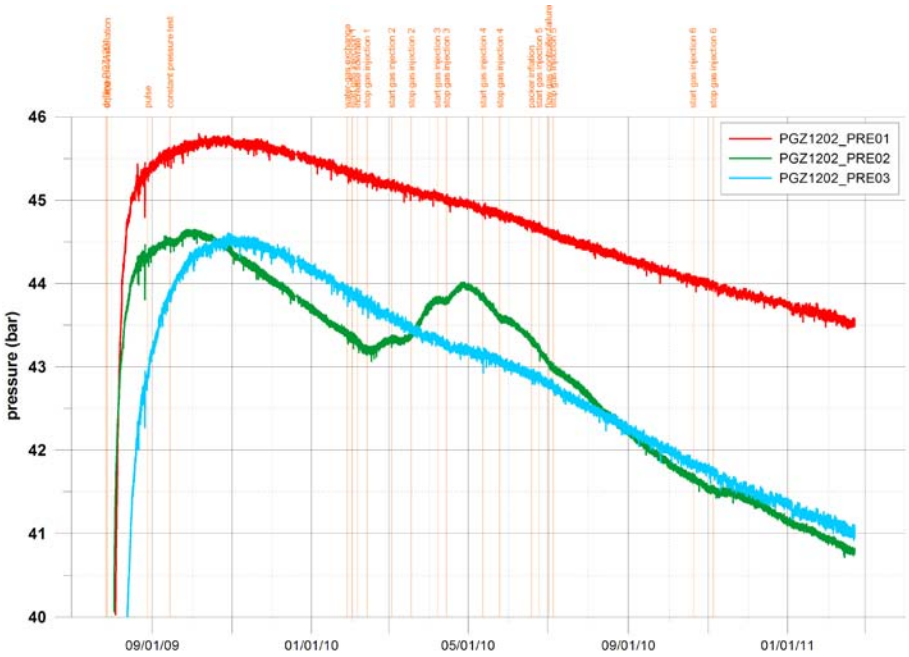

Figure 6 – *Water pressure in PGZ1202*

In PGZ1202 (Figure 6), we observe in PRE02 chamber a slight influence of gas injection. Of course this evolution is smoother than in PGZ1201.

We will mainly use pressure data from Figure 4 in PGZ1201 to assess quality of our numerical simulation presented in the following section. We will focus on pressure evolution in injection chamber PRE02 (i.e. Interval 2).

3. Description of numerical software Code_Aster and its conceptual models

Code_Aster (www.code_aster.org) is a numerical software developed by EDF which offers a full range of multiphysical analysis and modelling methods that go well beyond the standard functions of thermomechanical calculation code. In particular, Code_Aster deals with thermo-hydro-mechanical problems with partial saturation in porous media, including the gas transfers. However, in this report, the thermal problem will not be considered.

3.1 MODEL USED IN THIS STUDY

We consider a “HHM” (namely unsaturated biphasic Hydro-Mechanical) model. Details of Hydro-Mechanical models available in *Code_Aster* are given in [7]. Hereafter, we recall main equations of the model.

We present a setting for two-phase flow model. We consider 2 components (N_2 and H_2O), denoted by upper index *c* existing into 2 phases (liquid and gas), denoted by lower index *p*. In our study, we consider that there is no vapor ; hence water does not exist in gaseous phase. Gaseous phase is composed of nitrogen, liquid phase is composed of water and dissolved nitrogen.

Mechanical unknowns are displacements $u = (u_x, u_y, u_z)$. Hydraulical unknowns are liquid pressure $p_l = p_l^{H_2O} + p_l^{N_2}$ and gas pressure $p_g = p_g^{N_2}$. They are related by capillary pressure $p_c = p_g - p_l$. Capillary pressure p_c is related to water saturation S_l by Van-Genuchten relation:

$$S_{we} = \frac{1}{\left(1 + \left(\frac{p_c}{p_r}\right)^n\right)^m}$$

with

$$S_{we} = \frac{S_l - S_{wr}}{1 - S_{wr}}$$

where we have introduced

S_{wr}	Residual saturation
S_{we}	Effective saturation
p_r	Van Genuchten law parameter
m, n	Van Genuchten parameters such that $m = 1 - 1/n$

Liquid relative permeability is also given by Mualem Van-Genuchten model, such that :

$$k_r^l = \sqrt{S_{we}}\left[1 - \left(1 - S_{we}^{1/m}\right)^m\right]^2$$

Gas relative permeability is given by a cubic law ponderated by a coefficient C_k:

$$k_r^g = C_k\left(1 - S_l\right)^3$$

Nitrogen N_2 obeys to perfect gases law:

$$p_g^{N_2} = \frac{\rho_g^{N_2}}{M_{N_2}} RT$$

Where we introduce

ρ	density
M_{N_2}	Nitrogen molar mass

R	Perfect gas constant
T	Temperature

Two main equations govern system's evolution: balance momentum and fluid mass conservation. Balance momentum equation is

$$\nabla \cdot \sigma(u, p_c, p_g) = 0$$

Stress tensor is decomposed in effective stress tensor $\sigma^{'}$ and pressure stress tensor σ_p

$$\sigma(u, p_c, p_g) = \sigma^{'}(u) + \sigma_p(p_c, p_g)$$

Incremental form of pressure stress tensor reads:

$$d\sigma_p = -b(dp_g - S_l dp_c)$$

Where *b* designates Biot coefficient and S_l water saturation.

The variation of porosity $d\varphi$ is given by the classical eulerian representation

$$d\varphi = (b - .\varphi)\left(d\varepsilon_v + \frac{S_g dp_g + S_l dp_l}{K_S} \right)$$

With ε_v is volumetric strain and K_S the compressibility of the skeleton.

Mechanical behaviour obeys to Drucker-Prager's law. Material Young modulus and Poisson ratio are respectively denoted *E* and ν. Plasticity surface *F* reads

$$F = \sqrt{\frac{3}{2}} II_{\hat{\sigma}} + m\left(I_\sigma - \frac{3c}{\tan\phi} \right) = 0$$

where $II_{\hat{\sigma}} = \sqrt{\hat{\sigma}_{ij}\hat{\sigma}_{ij}}$ is second deviatoric stresses invariant, $\hat{\sigma}_{ij} = \sigma_{ij} - \frac{I_\sigma}{3}\delta_{ij}$ is deviatoric stresses tensor, $I_\sigma = \sigma_{ij}\delta_{ij}$ is first stresses invariant, coefficient *m* is given by relation $m = \frac{2\sin\phi}{3 - \sin\phi}$, ϕ is friction angle and *c* is cohesion. We notice that gravity effects are here neglected.

Mass conservation reads for component *c*:

$$\dot{m}_c + \nabla \cdot \left(F_l^c + F_g^c \right) = 0$$

where m_c (resp. F_l^c, F_g^c) designates mass inflow (resp. liquid, gaseous flux) of component *c*. For each phase, hydraulic fluxes obey to Darcy's law :

$$F_p = -\frac{k.k_r^p(S_l)}{\mu_p} \nabla p_p$$

k stands for anisotropic intrinsic permeability $k = (k_x, k_y, k_z)$, k_r^p for relative permeability and μ_p for dynamic viscosity of phase *p*.

Diffusion in liquid phase obey to Fick's law.

$$\frac{F_l^{H_2O}}{\rho_l^{H_2O}} + \frac{F_l^{N_2}}{\rho_l^{N_2}} = -D_l \nabla \rho_l^{N_2}$$

where D_l stands for Fick diffusion coefficient in liquid phase.

In the sequel, we will express D_l as a linear function of tortuosity τ, saturation and porosity such that:

$$D_l = S_l.\tau.\varphi \times D_{N2}^w$$

with D_{N2}^w the diffusion coefficient of nitrogen into water.

Water is slightly compressible, hence we have the relation

$$\frac{d\rho_l}{\rho_l} = \frac{dp_l}{K_l}$$

where coefficient K_l denotes water compressibility. Nitrogen dissolution obeys to Henry's law

$$\frac{\rho_l^{H_2}}{M_{N_2}^{ol}} = \frac{p_g^{H_2}}{K_H}$$

where K_H designates Henry's constant and $M_{N_2}^{ol}$ nitrogen molar mass.

3.2 SOME NUMERICAL ASPECTS

The previous problem is solved with finite elements with linear interpolation function for pressure and bilinear for the displacements. This choice is done to reduce oscillations and guarantees a better convergence. To ensure maximum principle and prevent oscillations in case of hydraulic shock , we use a method of "selective" mass matrix lumping. The selective method consists to separate integration points: on the vertex for the transient terms (lumping) and on the Gauss points for diffusion to avoid deteriorated results for those terms.

The treatment of gas appearance [3] is included in the choice of mains numerical unknowns: $(p_l, \chi_l^{N_2})$with

$$\chi_l^{N_2} = \frac{K_H \rho_l^{N_2}}{M^{N_2}}$$

Thanks to Henry's law, $\chi_l^{N_2} = p_g^{N_2}$ for an under-saturated medium. For a saturated one, $\chi_l^{N_2}$ is a function of nitrogen concentration in liquid.

4. Material data

In this paragraph, we give physical parameters that we use in following simulations.

Two materials will be simulated: the argillite and the injection chamber PRE02. The chamber is simulated by a porous media for numerical reasons. In the section 6, we will add a transient zone (damage zone).

4.1 ARGILITE

For argillite we use experimental data available in so-called "Dossier ANDRA 2005".

Hydraulic terms	
Intrinsic permeability	$k_x = k_y = 4.8.10^{-20} m^2, k_z = 4.8.10^{-21}\ m^2$ For the 2D and isotropic calcul: $k_x = k_y = k_z = 2.2.10^{-20} m^2$
Pondering factor of gas permeability	$C_k = 250$
Initial Porosity	$\phi^0 = 0.18$
Capillary curve	Van Genuchten model: $S_{wr} = 0$; $p_r = 15MPa$; $n = 1.49$
Liquid relative permeability	Mualem-Van Genuchten model
Gas relative permeability	Cubic law
Tortuosity	$\tau = 0.25$

Mechanic terms	
Young Modulus	$E = 4000MPa$
Poisson's ratio	$v = 0.3$
Biot coefficient	$b = 0.6$
Friction angle	$\phi = 15°$
Cohesion	$c = 3$ MPa

4.2 INJECTION CHAMBER PRE02 (INTERVAL 2)

One of the difficulties of this computation is to have a correct representation of the chamber. Due to the model, we are compelled to consider it like a porous and capillary medium.

Finally, we use the following parameters:

Hydraulic terms	
Intrinsic permeability	$k_x = k_y = k_z = 1.10^{-12} m^2$
C_k	$C_k = 250$
Initial Porosity	$\phi^0 = 0.25$ (corresponding to a volume in interval2 of 1,1 l)
Capillary curve	Van Genuchten model : $S_{wr} = 0$; $p_r = 0.01MPa$; $n = 1.49$ =

Liquid relative permeability	$k_r^l = 1$
Gas relative permeability	$k_r^g = 1$
Tortuosity	$\tau = 1$

Mechanic terms	
Young Modulus	$E = 1MPa$
Poisson's ratio	$v = 0.1$
Biot coefficient	$b = 0.99$
Compressibility	$\frac{1}{K_S} = 2.10^{-8} Pa^{-1}$

4.3 LIQUID AND GAS PARAMETERS

Water	
Viscosity	$\mu_l = 10^{-3} Pa.s$
Initial density	$\rho_l^0 = 1000 g.l^{-1}$
Compressibility	$\frac{1}{K_l} = 5.10^{-10}$ Pa
Gas (N_2)	
Viscosity	$\mu_g = 1.75.10^{-5}$ Pa.s
Henry coefficient	$K_H = 163934$ Pa. m^3/mol
Molar mass	$M_{N_2}^{ol} = 0.028$ g/mol
N2 Diffusion into water	$D_{N2}^w = 2.10^{-9}$ m^2 /s

5. Preliminary set of hypothesis of numerical simulations

5.1 GEOMETRY AND MESH

We present geometries and meshes used for numerical simulations presented in paragraph (3D) 5.5 and 5.6 (2D). We represent only PGZ1201 borehole. The axes (X,Y,Z) correspond to the direction of

principal stresses.

X : 65° North (GED direction, see *Figure 1*)

Y : 155° North

Z : Vertical direction

The angle between the borehole and the horizontal plane is $\theta = 35{,}4°$ (Figure 9) and the radius of the borehole is $r = 0.038m$.

1. 3D Mesh

In the sequel, we note (Figure 7) V1 and V2 the vertical faces, L1 and L2 the lateral faces and H1 and H2 the upper and lower faces. We consider only one half of the domain (and symmetric condition on vertical face V1,).

We will call B the boundary of the borehole and In the lateral face of the chamber.

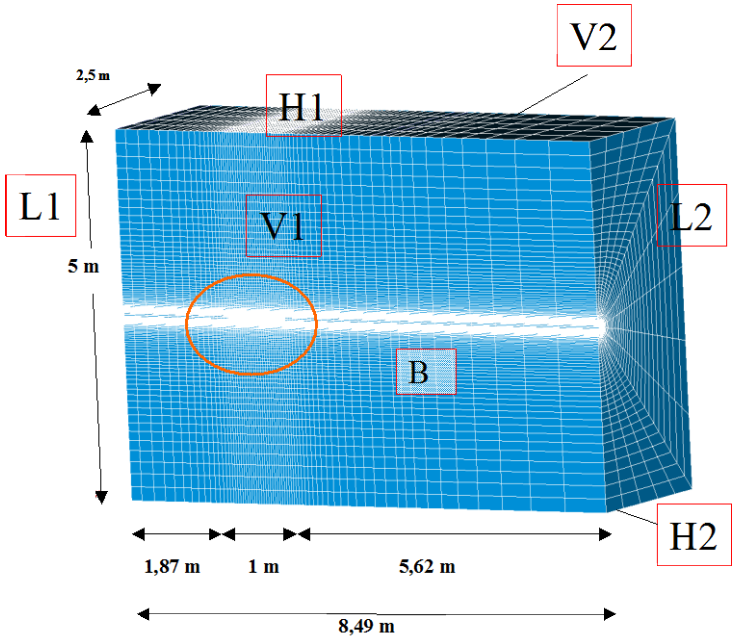

Figure 7 – *3D geometry with orange circled injection chamber*

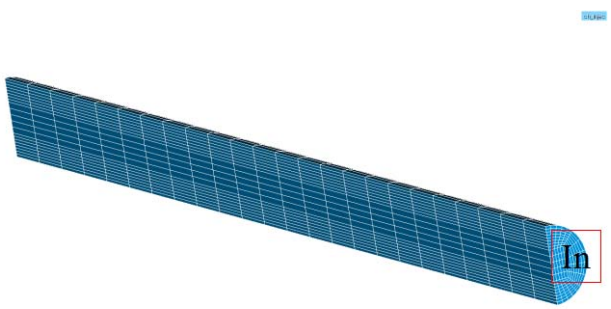

Figure 8 – *Zoom of injection chamber*

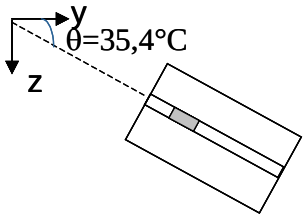

Figure 9 - *Orientation of the borehole*

Global mesh represented in Figure 7 is composed of 58560 hexahedra. Injection chamber is composed of 3480 hexahedra. 3D mesh fineness has been deduced from mesh sensitivity analysis leaded in dimension 2.

2. 2D Mesh

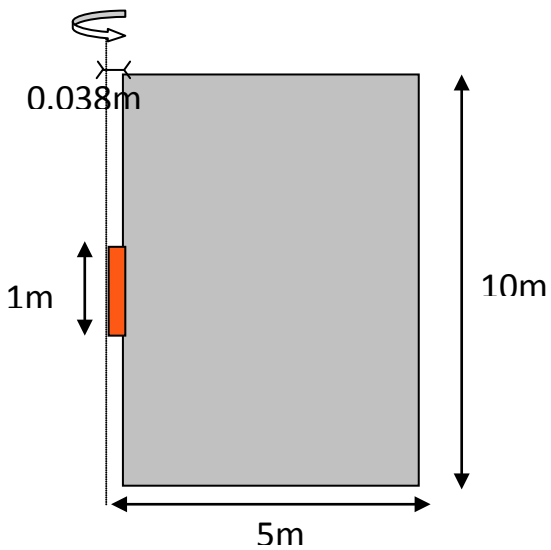

Figure 10 – *2D geometry with orange colored injection chamber*

2D mesh is composed of 21841 nodes and 10704 quadratic triangles. Injection chamber is composed of 3000 triangles. A parameter study on mesh refinement has been done in order to fit it: mesh convergence is obtained.

5.2 INITIAL CONDITIONS

The argillite is initially fully saturated, and the gravity is neglected. We consider that in the argillite the initial pressure is:

$$p_l^0 = 4{,}5MPa$$

The initial total stresses are the classical values used in the argilite and corresponding to the rocks weight:

$$\begin{cases} \sigma_{xx} = \sigma_h = -12.4MPa \\ \sigma_{yy} = \sigma_H = -16.1MPa \\ \sigma_{zz} = \sigma_v = -12.4MPa \end{cases}$$

For the 2D computation, we consider that:

$$\sigma_{xx} = \sigma_{yy} = \sigma_{zz} = -12MPa$$.

In the injection chamber, the medium is initially fully saturated and the liquid pressure is 1atm. Stresses are equal to 0.

5.3 STEPS OF SIMULATION AND BOUNDARY CONDITIONS

In this section, only the first 5 steps of gas injection have been simulated. The different steps of the computation could be summarized as follows:

Step	Duration	Event
1	1 h	Digging of the borehole
2	1day	Waiting
3	180 days	Installation of packers and chambers
4	4 days	Gas Injection GRI1a
	7 days	Gas Injection GRI1b
	19 days	Gas Injection GRIS1
	15 days	Gas Injection GRI2
	20 days	Gas Injection GRIS2
	7 days	Gas Injection GRI3
	28 days	Gas Injection GRIS3
	14 days	Gas Injection GRI4
	29 days	Gas Injection GRIS4
	11 days	Gas Injection GRI5
	107 days	Gas Injection GRIS5
	15 days	Gas Injection GRI6
	117 days	Gas Injection GRIS6

Table 1 – *Steps of simulation*

- **Boundary conditions common for all steps :**

On L1, H1, V2 :

- Hydraulic flows equal to zero
- Total normal stresses applied corresponding to initial conditions

On L2 :

- Hydraulic flows equal to zero
- Normal displacements equal to zero

On V1 (symmetry conditions):

- Hydraulic flows equal to zero
- Normal displacements equal to zero

- **<u>Boundary conditions for Step 1 :</u>**

On B (convergence confinement method):

- The total radial stress σ_r is decreasing from the initial radial stress σ_r^0 to 0.

$$\sigma_r = \sigma_r^0 \ .(1\text{-}t/(1h))$$

- The liquid pressure is decreasing from p_l^0 to 0.

$$p_l = p_l^0 \ .(1\text{-}t/(1h))$$

- **<u>Boundary conditions for Step 2 :</u>**

On B (consolidation):

- The liquid pressure is equal to p_l^0.

- **<u>Boundary conditions for Step 3 :</u>**

On B (consolidation):

- The liquid pressure is equal to p_l^0.
- Normal displacements equal to zero

On the boundary of the chamber :

- Hydraulic flows equal to zero
- Normal displacements equal to zero

- **<u>Boundary conditions for Step 4 :</u>**

On B (consolidation):

- The liquid pressure is equal to p_l^0.
- Normal displacements equal to zero

On the boundary of the chamber (except In):

- Hydraulic flows equal to zero

- Normal displacements equal to zero

On the lateral boundary In of the chamber :

- Normal displacements equal to zero
- Gas flow equal to gas injection : $F_g^c.n = Q_{inj}$.

The Gas flow is given in ml/min by Andra such as :

Flow rate's name	Begin (days)	End (days)	N_2 Flow (ml/min)
GRI1a	181	TGRI1A = 185	0,5
GRI1b	TGRI1A	TGRI1B=192	0,87
GRIS1b	TGRI1B	TGRIS1=211	0
GRI2	TGRIS1	TGRI2=226	1
GRIS2	TGRI2	TGRIS2=246	0
GRI3	TGRIS2	TGRI3=253	3
GRIS3	TGRI3	TGRIS3=281	0
GRI4	TGRIS3	TGRI4=295	1,5
GRIS4	TGRI4	TGRIS4=323	0
GRI5	TGRIS4	TGRI5=334	1,24
GRIS5	TGRI5	TGRIS5=441	0
GRI6	TGRIS5	TGRI6=456	1,24
GRIS6	TGRI6	TGRIS6=573	0

Table 2 – *Rate of gas injection*

The gas injection is expressed in *Code_Aster* in $kg/m^2/s$. According to injection's surface S such as $S = \pi r^2 = 0.00453 m^2$ and a nitrogen density $\rho_{N_2} = 1.14 kg/m^3$ we have the equivalence:

$$1ml/\min = 4.2.10^{-6} kg/s/m^3$$

5.4 EXPERIMENTAL CURVE CORRECTION

As said in section 2.1, an experimental drop of pressure is observed in PRE02 due to drainage of PGZ1031. In our computation this drainage is not taken into account and hydraulic phase will provide a liquid pressure equal to initial pressure (Figure 11).

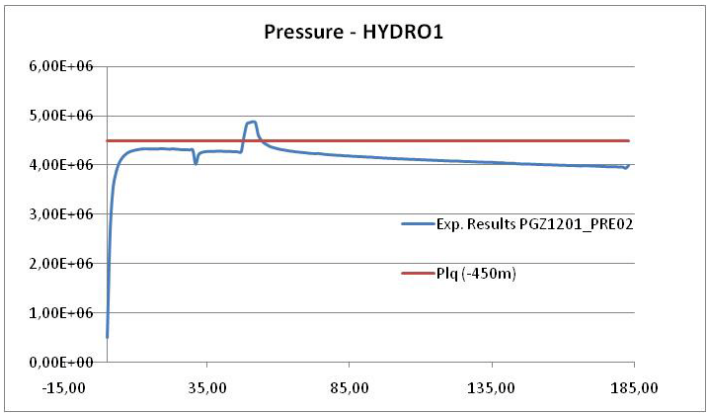

Figure 11 – *Experimental Pressure evolution for HYDRO1 Phase in injection chamber*

In order to make a convenient comparison between simulation and experimental results during GAS1 phase the experimental curve has to be corrected. Three ways to correct it are available (Figure 12):

1-A simple translation in order to have an initial pressure equal to 4,5 MPa at the beginning of gas injection (in red on the Figure 12)

2-A translation and a linear correction due to drainage considering that the drop of pressure due to drainage increases linearly with time (in green on the Figure 12)

3-A translation and a correction provided by R. De La Vaissière taking into account the drainage effect and the absorption of this effect observed experimentally (in brown on the Figure 12)

In the following, we will consider this last curve for the comparisons.

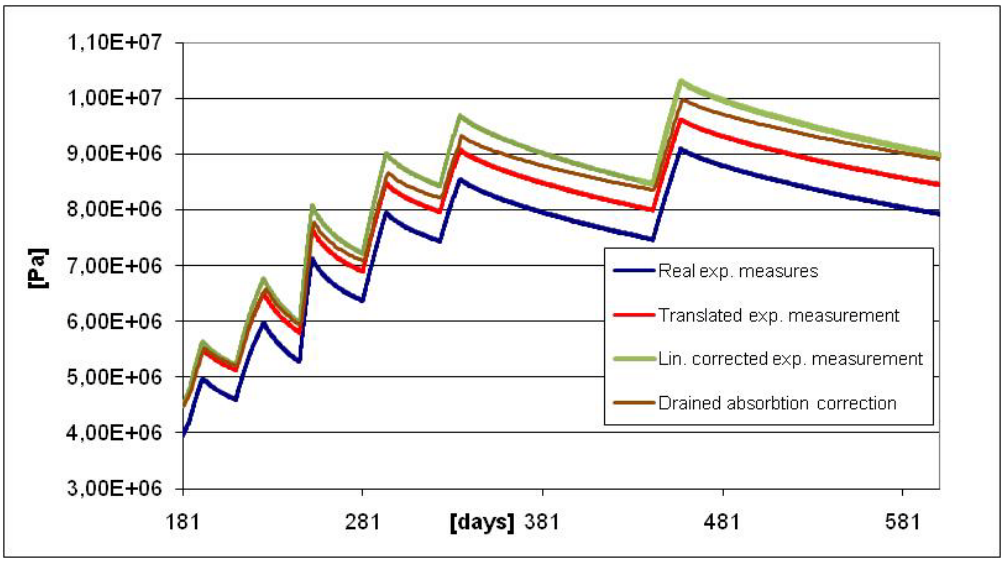

Figure 12 – *Corrections of experimental Pressure measurement in injection chamber during GAS1*

5.5 3D COMPUTATION

We will present pressure evolution in the three measurement's interval of PGZ1201: PRE03, PRE02, PRE02. These intervals are represented in the computation by 3 points (Figure 13).

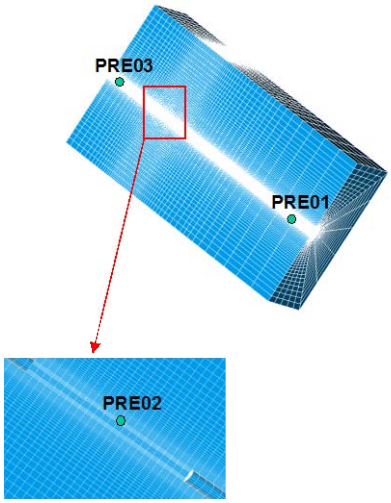

Figure 13 - *Measurement points*

3. Time evolution in PGZ1201 borehole

We present the liquid pressure evolution for the 3 intervals. As expected, the pressure does not change in both intervals PRE01 and PRE03, those intervals are too far from the injection chamber and no borehole damage zone allows the fluid to go through. In the sequel we will focus only on PRE02 and on the GAS1 phase (Figure 15 for liquid pressure and Figure 16 for saturation). We can observe two main trends: for the 3 first steps of injection the differences between numerical and experimental results are quite small. Indeed, we can suppose that with a better fitting of the parameters (cf. 2D computations) the results will be similar. For next steps, curves deeply differ: the experimental pressure continues to increase while the numerical one decreases. These decrease seams quite logical with our hypothesis and follows the quantity of gas injected. Indeed after TGRI3 the gas flow is smaller. If we are looking at the saturation evolution in the chamber (Figure 16) we simultaneously observe pressure decrease and a desaturation of chamber. Before TGRI3, nitrogen is entirely dissolved into the water in the chamber.

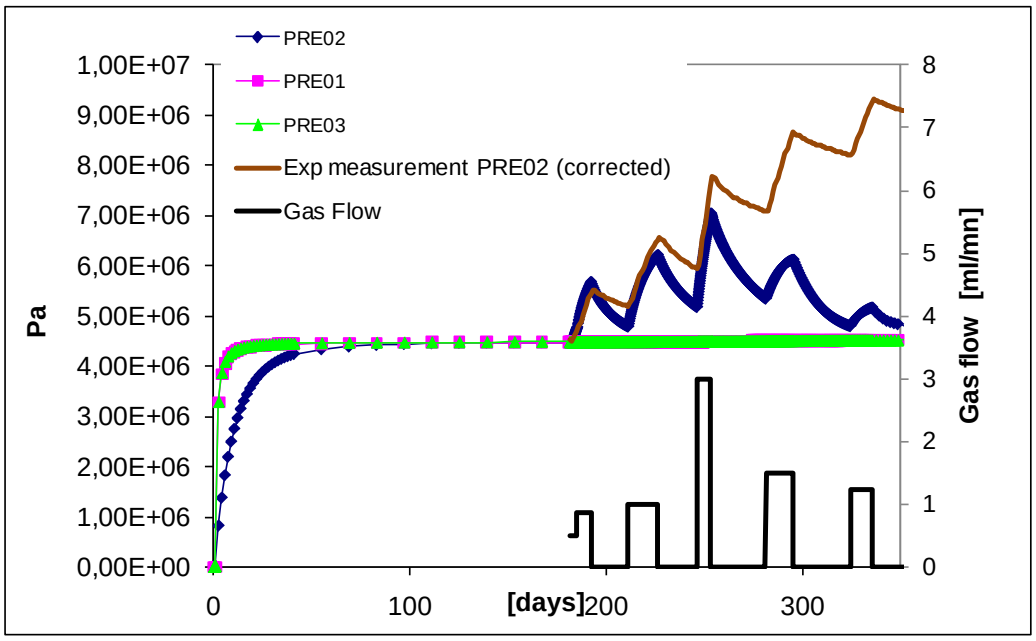

Figure 14 - *Liquid pressure evolution*

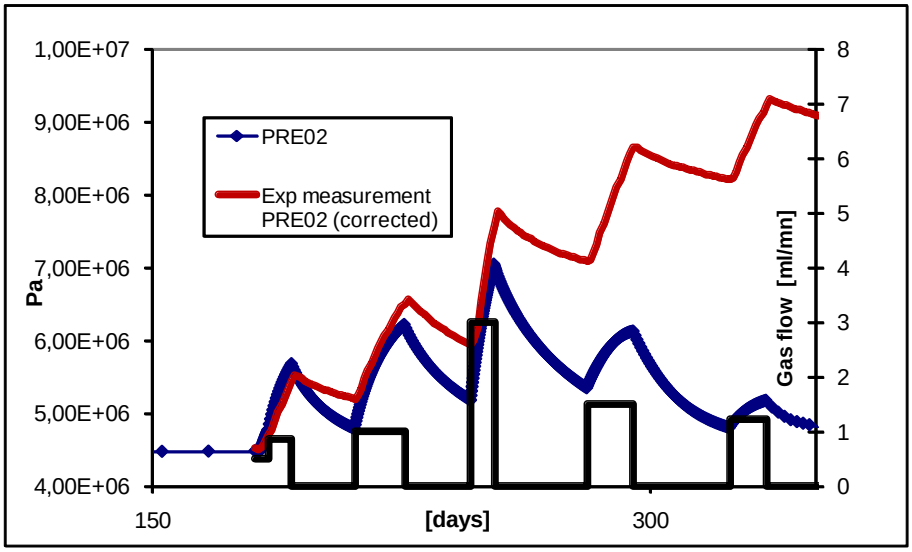

Figure 15- *Liquid pressure evolution, zoom on GAS1 phase*

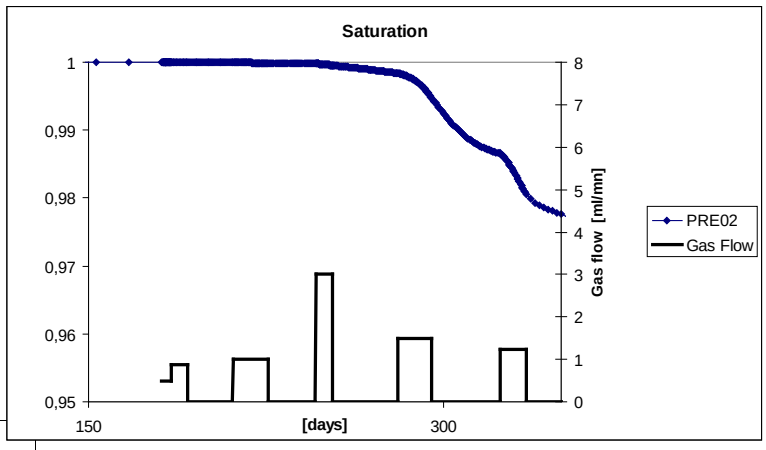

Figure 16 - *Numerical saturation evolution*

4. Isovalues

We see on Figure 17, Figure 18, Figure 19 and Figure 20 the liquid pressure isovalues for the different time steps (TGRI1, TGRI3, TGRI4, and TGRI5). We observe that the influence zone of the gas is very small and close to injection chamber. We also observe that the effect of anisotropy is very weak. Hence all the following computations will be done in 2D.

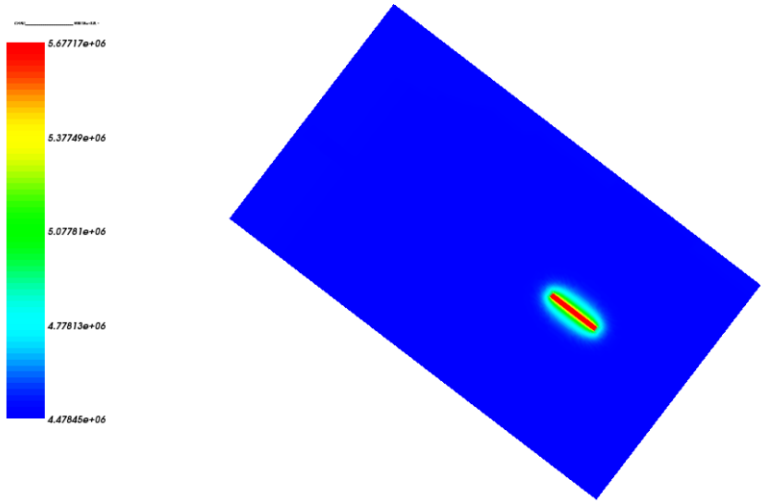

Figure 17 - *Liquid pressure isovalue at t = GRI1*

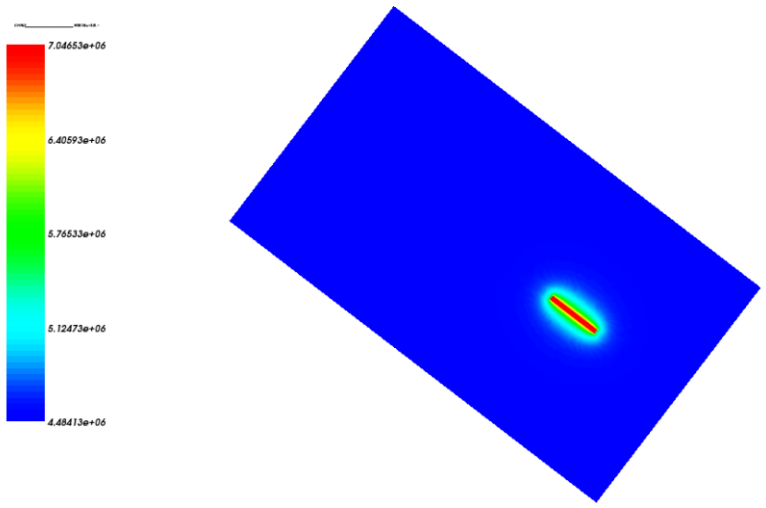

Figure 18 - *Liquid pressure isovalue at t = GRI3*

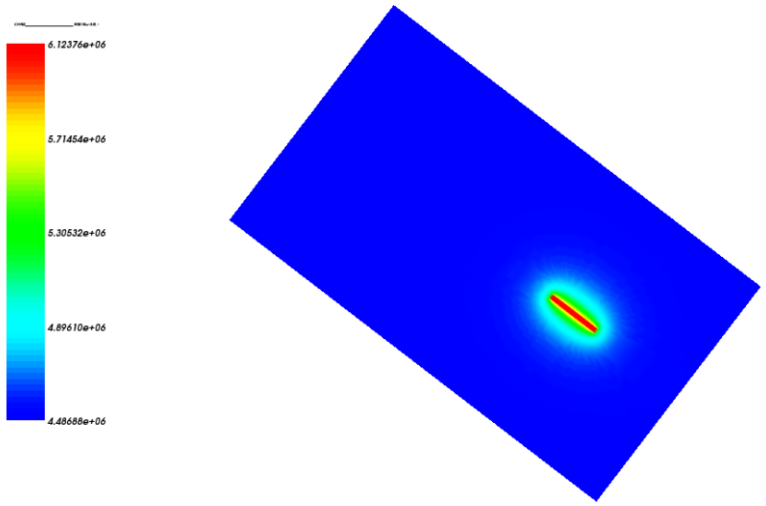

Figure 19 - *Liquid pressure isovalue at t = GRI4*

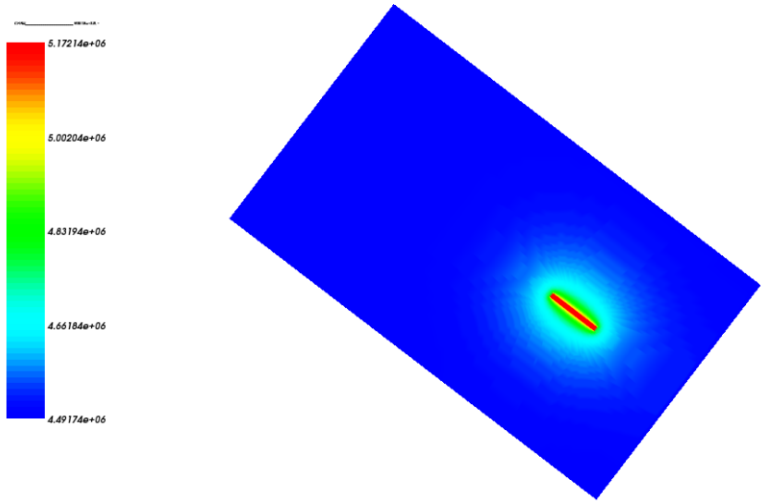

Figure 20- *Liquid pressure isovalue at t = GRI5*

5.6 AXISYMETRIC COMPUTATIONS

2D computations allow us to provide several computations and parameter studies. In the following we will give the time evolution of values on PRE02 and if required some profiles along an horizontal line L (Y=4,5m).

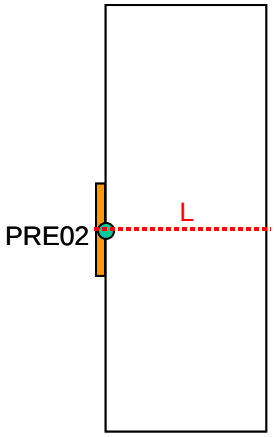

Figure 21 - *Point and line of post-processing on 2D model*

i. Reference computation

We remind that for 2D modeling, we use $k_x = k_y = k_z = 2.2.10^{-20} m^2$. We present on Figure 22 the liquid pressure evolution on PRE02.

The experimental results is very well fitted until the third gas injection steps (t = TRGI3). This comforts the hydraulic parameters chosen for the undisturbed clay. As for the 3D computation, after TGRI3, the curves deeply differ: the experimental pressure continues to increase while the numerical one is decreasing. This is corresponding to a desaturation of the injection chamber (Figure 23) and a change of mechanism.

Looking at the evolutions on the line L at several times of liquid pressure, gas pressure (or Nitrogen concentration, cf.3.2) and liquid saturation respectively on Figure 26, Figure 27 and Figure 28, we observe that there is no desaturation of the clay. The Nitrogen is only transported in the rock by a dissolution diffusion phenomena on a area less than 30cm. This is confirmed by the isovalues of $\chi_l^{N_2}$ (Figure 29) showing that the zone of nitrogen diffusion is very small and close to the chamber. This is consistent with the experimental results showing no evolution on PRE01 and PRE03 (Figure 4).

Concerning the mechanical evolution: we are looking at the values on the line L at several times. The radial stresses Figure 24 stay in compression: no breakdown is envisaged. A small (< 2cm) plastic zone appears after excavation (Figure 25) and does not increase. As expected and with such a model after (with simplified hypothesis of perfect plasticity), the gas does not affect the damage zone. The coupling with mechanic is weak here.

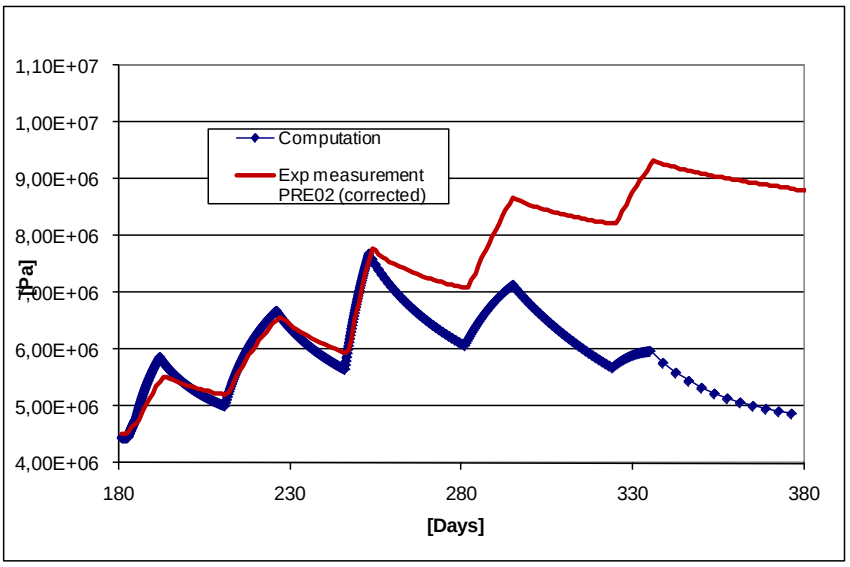

Figure 22 - *Liquid pressure evolution on PRE02*

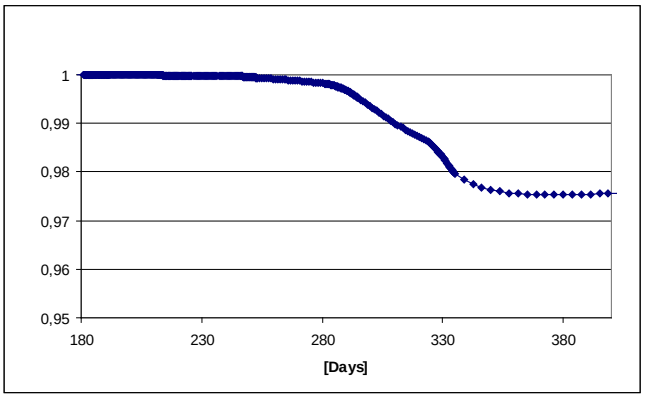

Figure 23 - *Saturation evolution on PRE02*

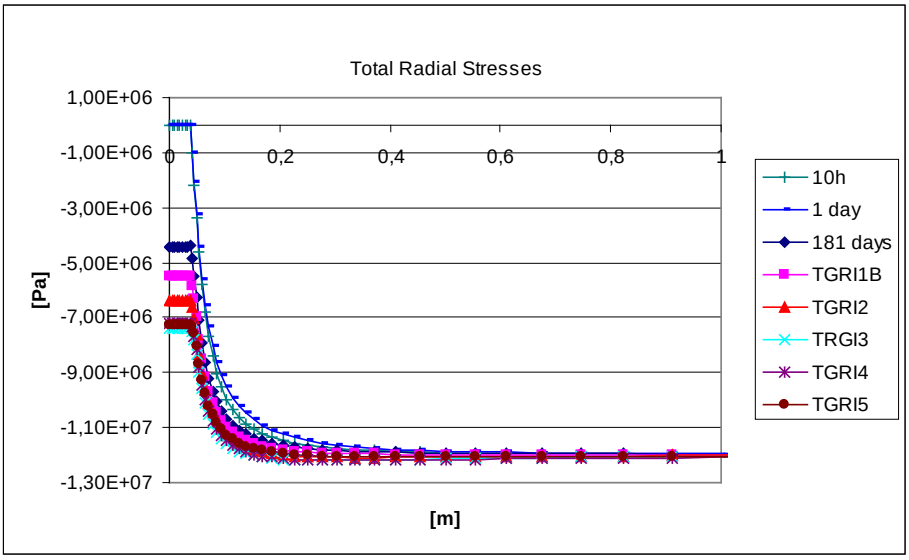

Figure 24 - *Total radial stresses at several times along L*

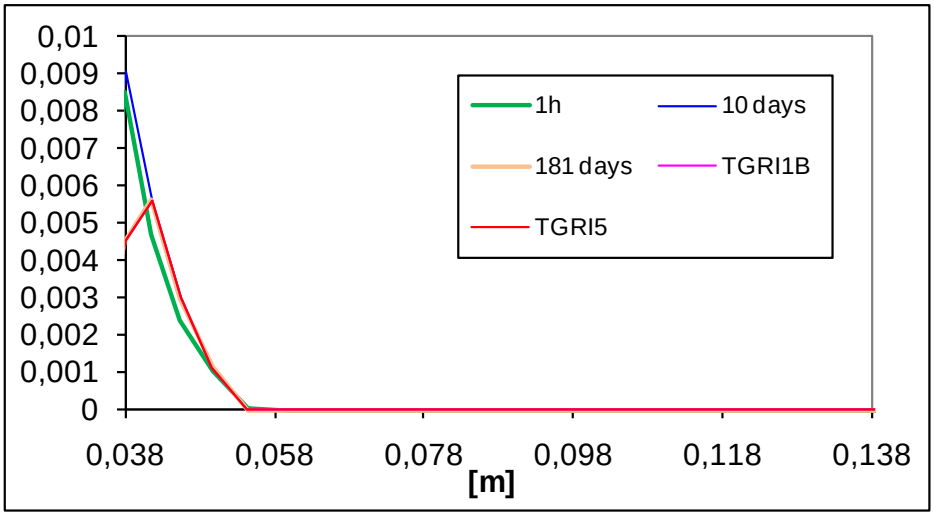

Figure 25- *Plastic strain at several times along L*

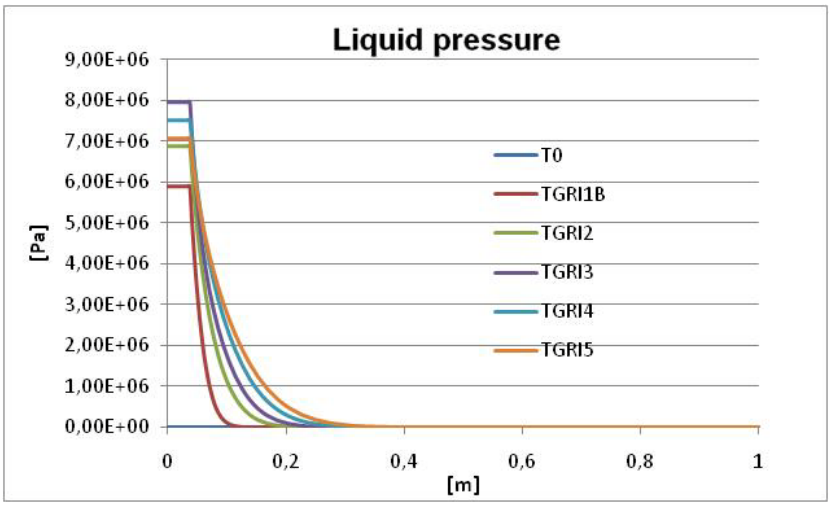

Figure 26- *Liquid Pressure at several times along L*

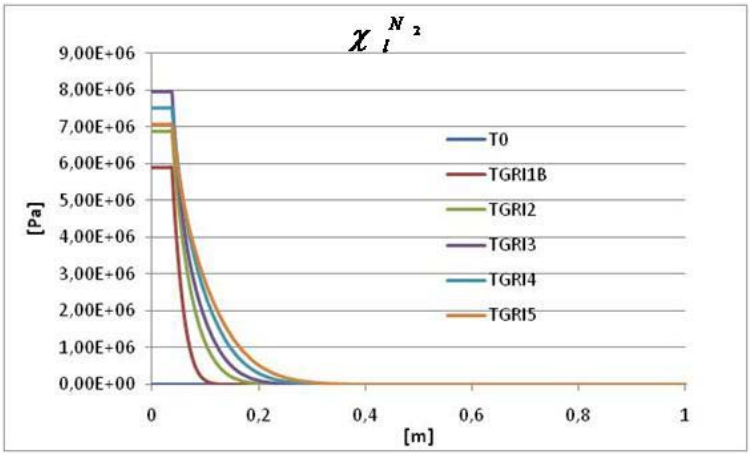

Figure 27- $\chi_l^{N_2}$ *(Gas pressure or concentration) at several times along L*

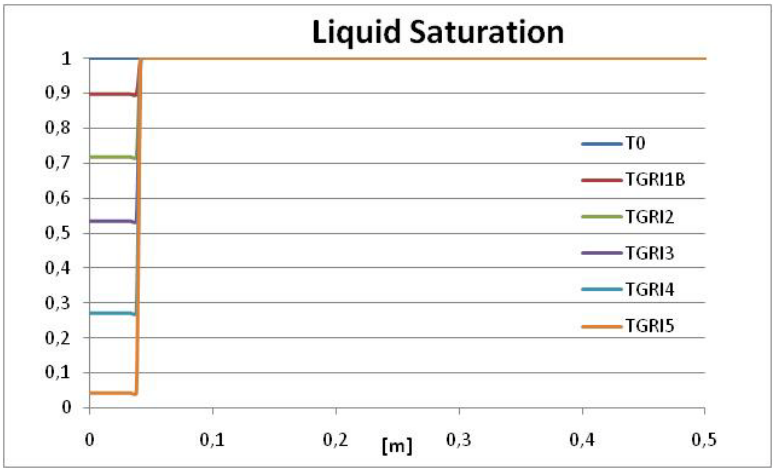

Figure 28- *Liquid Saturation at several times along L*

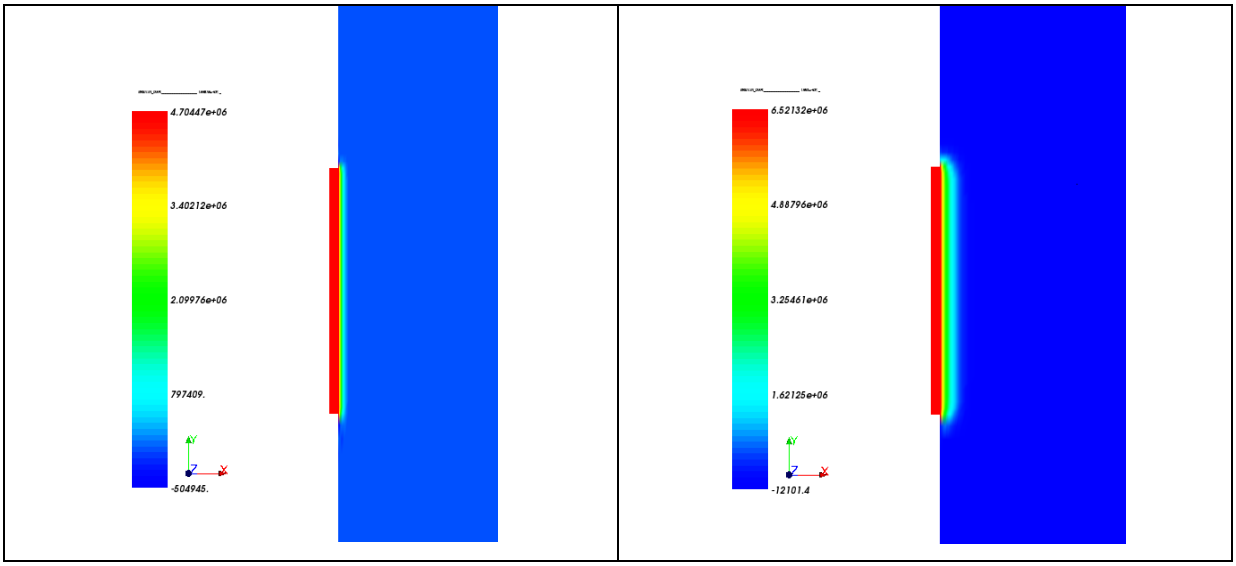

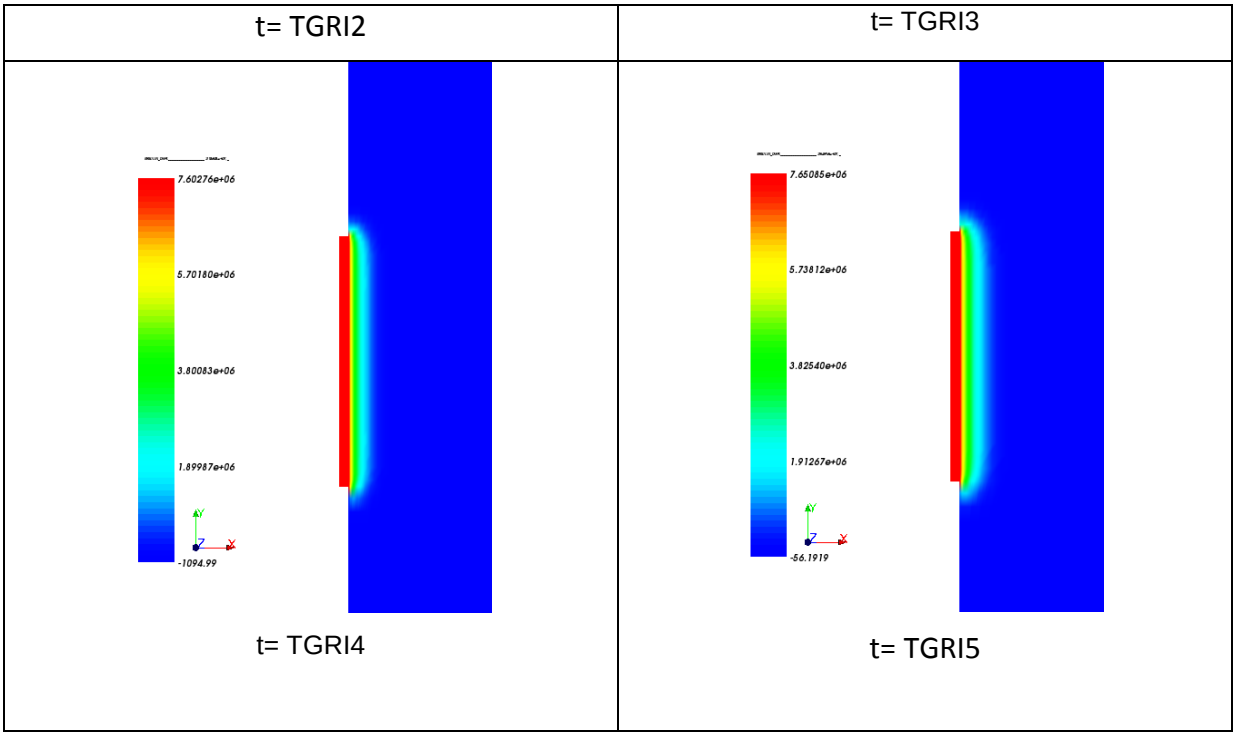

Figure 29 $\chi_l^{N_2}$ *isovalues (zoom around the chamber)*

ii. Influence of chamber compressibility

One of the encountered difficulties is the modeling of injection chamber. For numerical reasons we have to represent this “void material” by an equivalent porous media which is not obvious to calibrate : we have to introduce hydraulic parameters (such as capillary pressure) and to determinate its compressibility. This last one is unknown but has a high influence on the result. We can see on Figure 30 a comparison between two compressibilities: if we consider the 3 first steps this data has an influence on maxima of gas pressure (linked by dotted lines), but not on minima .

The fitting of this value is very important to understand what happens in argilite. It enhances the importance and the difficulty to modelize the non porous media instrumentation material (see also section 6.7).

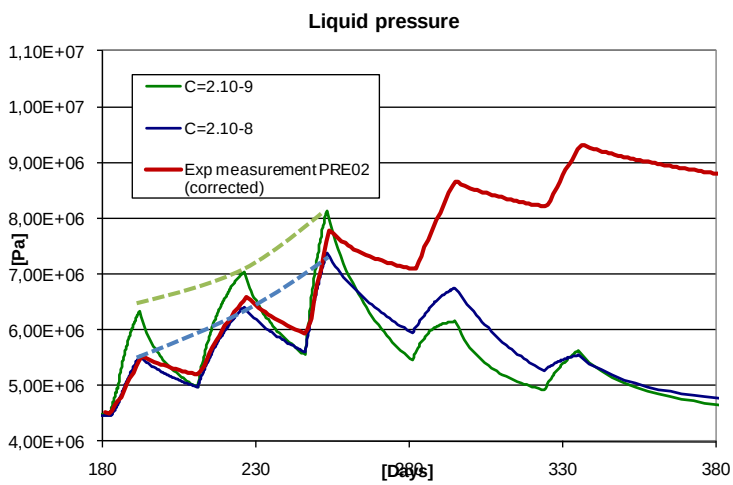

Figure 30 - *Influence of chamber compressibility*

iii. Influence of argillite permeability

Figure 31 shows the liquid pressure evolution obtained on PRE02 with two different permeabilities: $k_x = k_y = k_z = 1.10^{-20}\,m^2$ (noted $K = 1.10^{-20}\,m^2$) and $k_x = k_y = k_z = 2.410^{-20}\,m^2$ (noted $K = 2.4.10^{-20}\,m^2$). Of course, more the permeability is small and more the pressure is high. We can notice the influence of permeability on each pressure minima (followed by dotted lines on the figure). It is obvious that only one permeability in the rock will not be sufficient to fit the experimental curve.

A good way to fit the experimental curve is to change the argillite permeability after t=GRI3 :

$$t < GRI3 \quad k_x = k_y = k_z = 2{,}2.10^{-20}\,m^2$$
$$t > GRI3 \quad k_x = k_y = k_z = 2.10^{-21}\,m^2$$

With this hypothesis, we can observe on Figure 32 that experimental results are correctly fitted. Nevertheless, this case is clearly unrealistic. Indeed reducing the permeability means a self healing of the rock during the gas injection which is not reasonable. The question is here to understand the reason of this change of state.

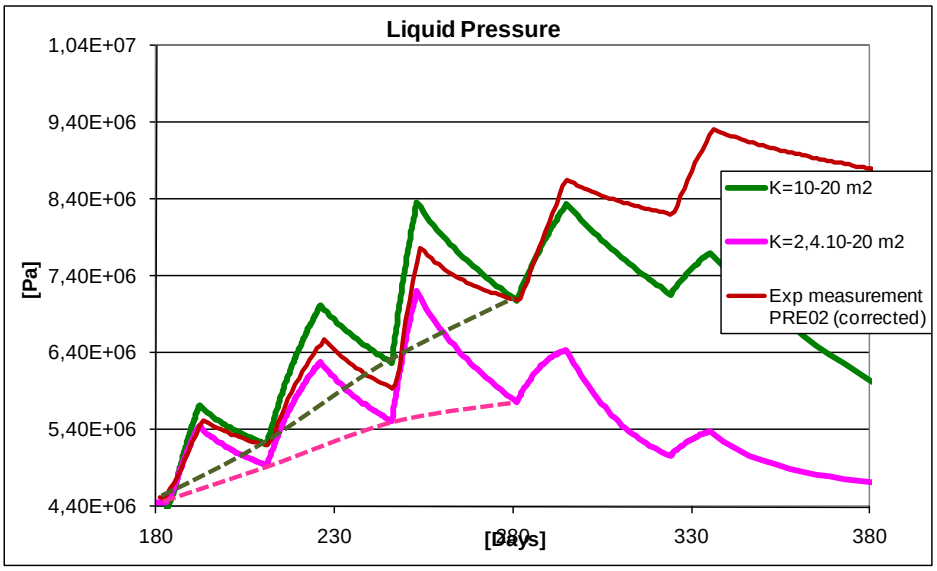

Figure 31 - *Influence of undisturbed rock intrinsic permeability*

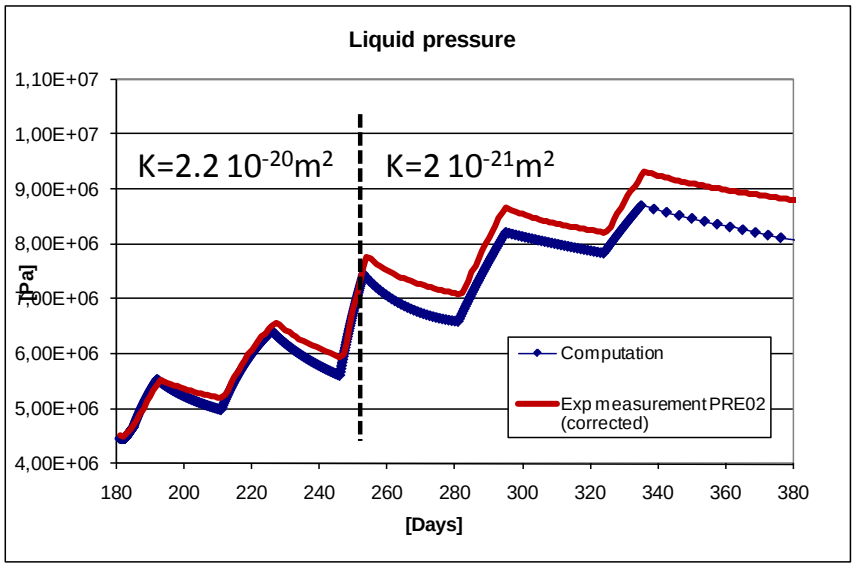

Figure 32 - *Modification of rock permeability after GRI3*

6. Second set of hypothesis of numerical simulations: taken into account of the initial saturation of the injection interval

6.1 SOME ELEMENTS CONCERNING THE VOLUME OF THE INJECTION'S CHAMBER

In [4] and [5] an analysis of the volume of vacuum Interval 2(Figure 33) is provided and gives more precisions. This volume is composed of an "incompressible" volume (corresponding to the case of a full convergence around the filter) and of a part corresponding to a void around this filter. This void will be filled up during the convergence of the rock. Knowing that, the theoretical volume of vacuum in interval 2 ranges between 804 cm^3 and 1540 cm^3.

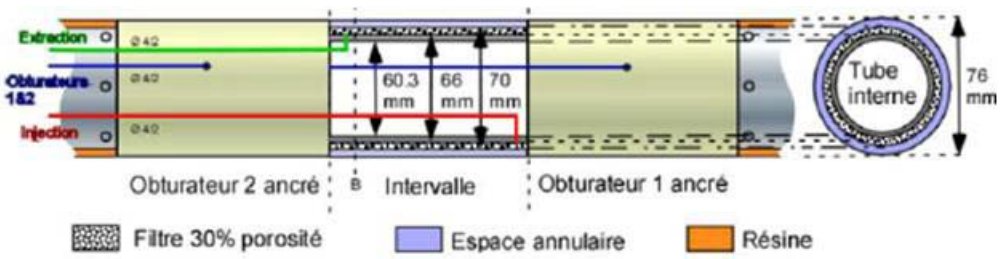

Figure 33 – *Interval 2 (injection chamber)*

Moreover, the volume of water rejected by flushing in the interval during the water-gas exchange before GAS1 phase is equal to 810 cm^3. This volume corresponds to the initial volume of gas in the chamber before injection.

At least, in [5] the pressure differential is fitted by an analytical solution at constant volume using a Perfect Gas law. The best fitting before GAS1 is obtained with a volume of 1040 cm^3. This gives us an indication of the volume of interval at the beginning of injection. After that, the fitting is done for each injection steps: the gas volume increases and becomes more important than maximum theoretical value (1540 cm^3) of interval volume after GRI3. An interpretation of that is that residual water is first rejected, and then that gas penetrates in the rock but more and more hardly.

In the first set of hypothesis presented in section 5, the chamber is fully saturated before gas injection due to hydraulic phase. This is not consistent with the observation done before. In the following, new computations are done only for Gas 1 phase considering a volume of 1040 cm^3 for the interval 2. Initial saturation of gas will be taken into account.

Of course, a lot of approximations will be done: first, convergence of rock is not taken into account; secondly the chamber is, for modeling reasons, represented by a porous media which is of course false. How wrong are we, doing this, is a crucial question.

6.2 NEW HYPOTHESIS OF COMPUTATION

Mesh and geometry are the same than in section 5.6 (axisymmetrical computation). Volume of the chamber is equal to 1040 cm^3 ($\phi^0 = 0{,}23$). Only GAS1 phase corresponding to Table 2 is modelled. For this section, the 6 steps of injection are available and modelled.

- **Initial condition in argillite :**

As in [5] the argillite is initially fully saturated, and the gravity is neglected. The initial pressure is:

$$p_l^0 = 4{,}5MPa$$

- **Initial condition in interval 2 :**

The saturation is such as:

$$S_l = 1 - \frac{810}{1040} = 0{,}22$$

According to the van-genuchten parameters indicated in section 4.2, it provides an “artificial capillary pressure” $p_c^0 = 0{,}021MPa$

We consider water equilibrium and $p_l^0 = 4{,}5MPa$

6.3 REFERENCE COMPUTATION

For this computation, in the host rock we take $k_x = k_y = k_z = 4.10^{-20} m^2$. All the other data are the same than in section 4. In this section, we only consider undisturbed host rock (without BDZ).

Gas pressure evolution with these hypotheses is presented in Figure 34 with the red curve. Until second injection step (≈2 30 days), experimental results are well reproduced, afterwards, differences are consequents.

The blue curve represents the same computation but with a chamber initially partially saturated (0,9). Logically, the pressure is much higher (and this, as the first step of injection). Looking at the profiles on the line L_h at several times of gas pressure and liquid saturation respectively Figure 35 and Figure 36, we observe that penetration of gas remains located near the injection interval: influence area is less than 20cm. The saturation stays high (more than 0,95). Looking at the ratio between gas and liquid nitrogen volume on Figure 38, we confirm that even in this case, most of nitrogen is transported by dissolution/diffusion.

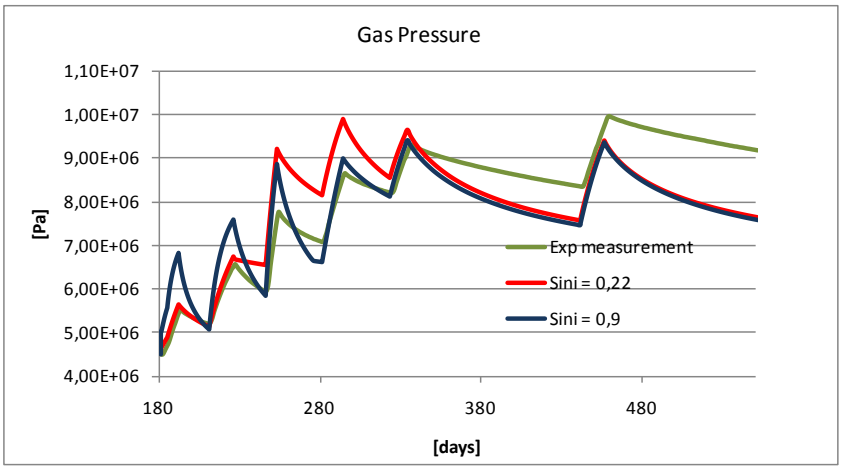

Figure 34 – *Gas pressure evolution in interval 2: goal of initial saturation*

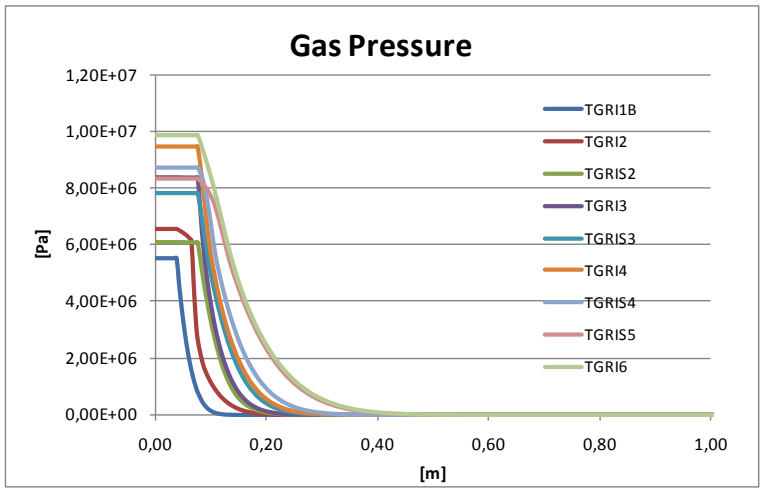

Figure 35 – $\chi_l^{N_2}$ *(Gas pressure or concentration) at several times along L*

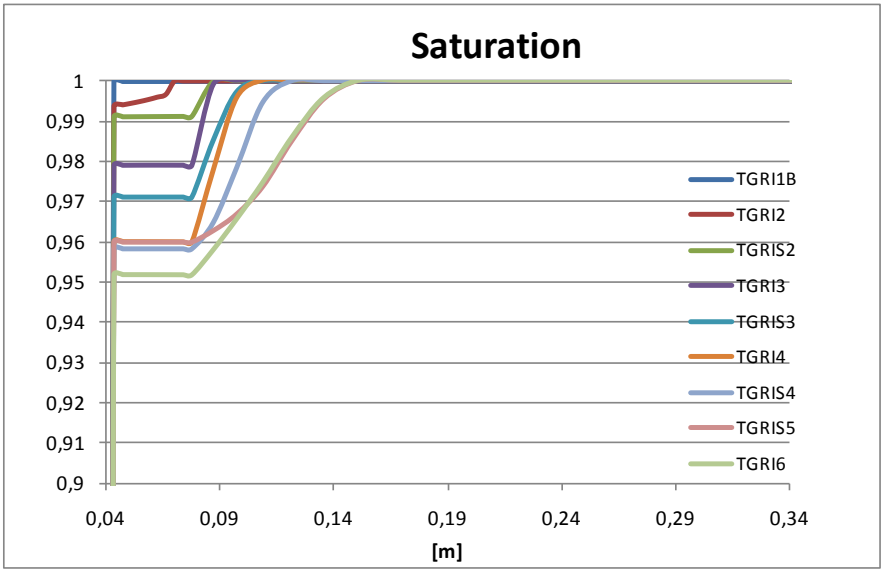

Figure 36 – *Liquid Saturation at several times along L*

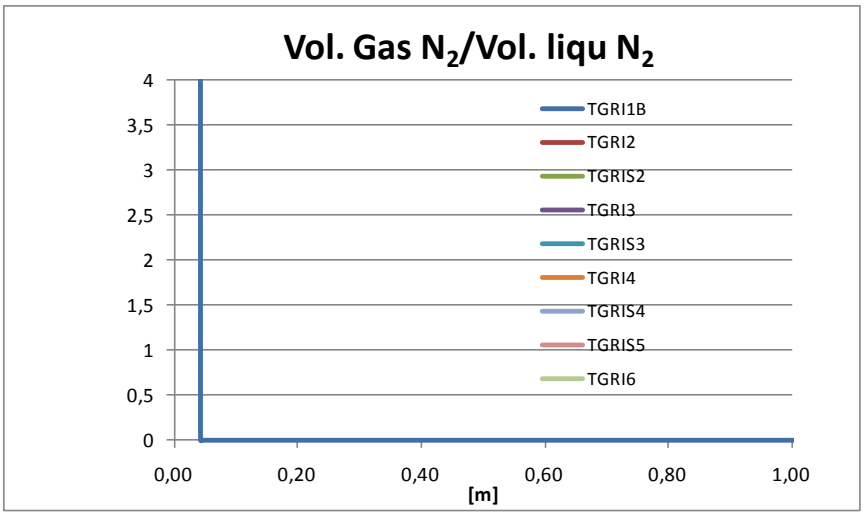

Figure 37 – *Gas/liquid ration of Nitrogen at several times along L*

6.4 INTRODUCTION OF A BOREHOLE DAMAGE ZONE

A borehole damage zone (called BDZ) is now introduced. We take a radius equal to the radius of the hole (3,8 cm, larger than the 2cm found in section Figure 25). Considering that no pressure evolution is observed in chamber PRE01 and PRE03 (Figure 5), we can imagine that this damaged zone has been closed around the packer by swelling of this one. The hypotheses we choose are summarized in Figure 40. We call this area "borehole damage zone" because we can imagine that there is an area due to drilling (Figure 25), but this area could also be a "transient zone" mixed of a damage zone and materials produced by injection gas (mud, gel, etc.).

Figure 41 shows pressure evolution in interval 2. We can observe that results with or without BDZ differ very weakly until 230 days. In this part, we can suppose that injection chamber behavior plays the main role and that water removal is the major phenomena. After 230 days,

the results obtained with BDZ are better than those without: this damage zone seems to play an important role. Results are in very good agreement with experimental results until the begin of third injection step, after they differ. Nevertheless, after this, differences between results with and without BDZ seem to remain more or less constant.

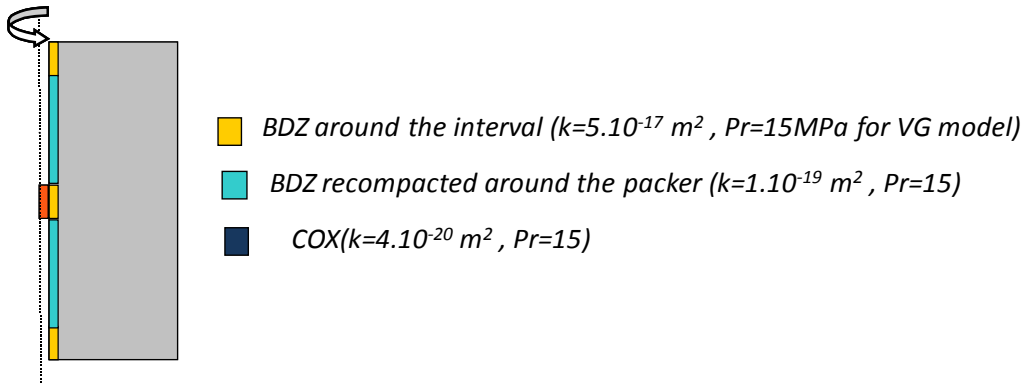

Figure 38 –*Configuration and hypothesis of modeled BDZ*

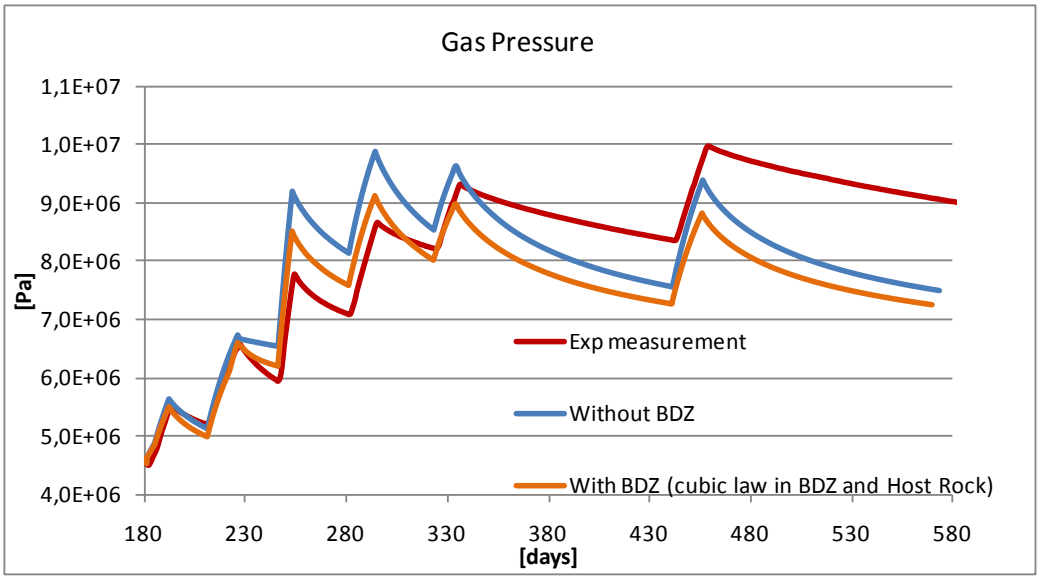

Figure 39 – *Gas pressure evolution in interval 2: goal of BDZ*

6.5 GOAL OF GAS PERMEABILITY IN HOST ROCK

As written previously and according to several experimental results, we take for argillite a cubic law for gas permeability law. This law is not precisely known and we propose here a sensitive analysis.. For that, we change the cubic law in the undisturbed host rock by a quadratic law: $k_r^g = C_k(1-S_l)^4$.

In BDZ, the relative permeability remains a cubic law. All the other data are the same than previous.

According to Figure 46, we observe that this parameter is not influent for the 4 first steps of injection. After that differences are significant. We can interpret that, according with time, each

material is successively predominant: injection chamber, then BDZ and finally undisturbed host rock.

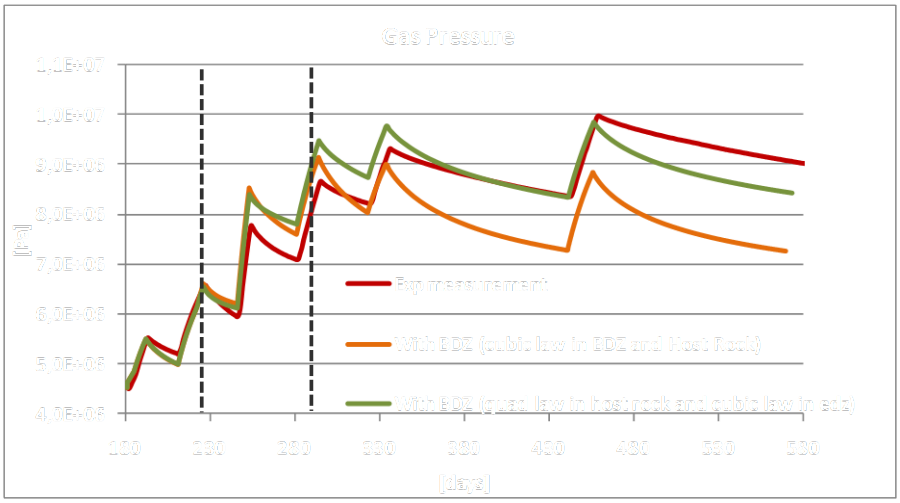

Figure 40 – *Gas pressure evolution in interval 2 : goal of relative permeability in host rock*

7. Conclusions

This contribution proposes a numerical modeling of a field scale test with a classical coupled two-phase flow model. The major difficulty in experience modeling is finally to understand and capture what happens in the instrumentation process and not only as far as the undisturbed clay is concerned.

By the way, we can more or less reproduce experiment and provide an interpretation of involved mechanism. Indeed, we suppose that different phenomena play successively a role: First, injection chamber comportment is predominant and we observe essentially water displacement, secondly, the borehole damage zone plays a prominent part and at least undisturbed host rock seams to become the leader.

In both simulations and experimental results, we observe that the gas influence zone is very small. In undisturbed host, no désaturation is observed.

We can see that even for PGZ1 (expected as a test in a undisturbed host rock), damage zone plays an important goal. This small zone is complex to estimate a priori because not only due to digging. A better characterization of this damage zone (suction, gas permeability, etc.) seems to be necessary to obtain a better fit of experimental results and predictive computations.

8. References

[1]Tests hydrauliques dans le forage de l'unité de programme PGZ1 en galerie GED. Forage PGZ1201 et PGZ1202. Rapport d'opération. Document ANDRA D.RP-OCPE.09.0028, 10/05/04

[2]Code_Aster, **www.code-aster.org**.

[3]Angélini, O. Chavant, C. Chénier, C. Eymard, R. Granet, S. "Finite Volume Approximation of a Diffusion-dissolution model and application to nuclear waste storage", *Mathematics & Computers in simulation* 81(10): 2001-2017 (2011).

[4]De La Vaissière, R. Talandier, J. « Gas entry pressure in Callovo-oxfordian claystone : in situ expermiment PGZ1 » Acte du colloque national Transfert 2012, ECL/LML 2012.

[5]De La Vaissière. Expérimentation PGZ Analyse de la phase d'injection de gaz GAS1. Document Andra D.NT. AMFS.11.0084

[6] P.Gerard, R.Charlier, F.Collin, R.Fernandes, S.Granet, D.Arnedo, S.Olivella, Description of initial numerical codes and conceptual model (undisturbed and disturbed host rocks). Forge Project – Deliverables 4.5 and 5.5 (February 2010).

[7]S. Granet, Modèles de comportement THHM, doc R7.01.11, available on **www.code-aster.org**.

[8] Coussy O. 2004. *Poromechanics*. Wiley, London.

Annexe 1

Formular

TESTING PLAN FOR 3-FOLD PACKER SYSTEM

SOLEXPERTS

LSMHM: Expérience PGZ						*Date*	12.08.2009	*Responsible / version*	PA / inst
Borehole	*PGZ 1201*	*Direction*	-30°	*Reference point*	Borehole head	*JOB Nr*	1752-12	*Location*	LSMHM Bure
Borehole Depth	28.51 m	*Stickup*	-0.350 m	*Borehole diameter*	76.00 mm	*Pressure Packer*	**180 bar**	*System*	*PRERGT_03_30*

Note: All depths shown are not correct for borehole deviation

- Packer, inox (4/2.4 mm)
- Pressure, inox (4/2.4 mm)
- Circulation Int.1&3, inox (4/2.4
- Circulation int.2, inox (1/4 ")
- Resin inj., polyamid (6/4 mm)
- Resin extr., polyamid (6/4 mm)

Lines
injection line
interval 2 = 1/4"

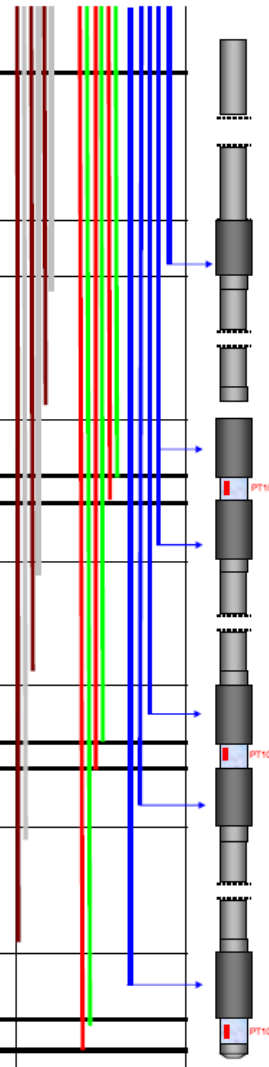

				Qty -	L_{unit} mm	L_{total} m	Depth m	OD mm	ID mm	*Comments:*
Stickup	-0.350 m bgl									Stickup < 0 means out of borehole
Reference							0.00			Reference vertically from mark
RODS				Rods with connector						*VOLUMES calculation:*
				1	1090	1.09				Filter inner tube OD: 66 mm
				0	0	0.00				V_{resin} (interv) = 1.68 L/m
							0.746			V_{resin} (lines 6/4) = 0.013 L/m
PACKER 6		Pa6			484			72		V_{eau} (interv 1 m) = 0.750 L
							1.230			
RESIN 3				Rods with connector				60.3		37.56 L
				1	129	0.13				
				9	2416	21.74				
				1	129	0.13				
							23.232			
PACKER 5		Pa5			484					
INTERVAL 3	PGZ1201_PRE_03	Q3 P3	PT1000		212		23.716	72	66	0.41 L
	+ PGZ1201_TEM_03						23.928			
PACKER 4		Pa4			484					
							24.412			
RESIN 2				Rods with connector				60.3		0.99 L
				1	220	0.22				
				0	0	0.00				
							24.832			
PACKER 3		Pa3			984					
INTERVAL 2	PGZ1201_PRE_02	Q2 P2	PT1000		1000		25.616	72	66	1.26 L
	+ PGZ1201_TEM_02						26.616			vol intervalle: 751 ml
PACKER 2		Pa2			984					vol lignes: 510 ml
							27.600			
RESIN 1				Rods with connector				60.3		1.07 L
				1	220	0.22				
				0	0	0.00				
							27.820			
PACKER 1		Pa1			484					
	+ PGZ1201_TEM_01						28.304	72		
INTERVAL 1	PGZ1201_PRE_01	Q1 P1	PT1000		186		28.490		66	0.51 L
	End cap				20					
	End Borehole						28.510			